

Article

High Temperature Tribological Behavior of Electroless Plating Ni-P-Si₃N₄-WS₂ Composite Coatings

Xiaohua Zheng¹, Yindi Huang^{1,*}, Chenbin Cai¹, Haijun Huang² and Fang Yang¹¹ College of Materials Science and Engineering, Zhejiang University of Technology, Hangzhou 310014, China² Zhejiang Testing & Inspection Institute for Mechanical and Electrical Products Quality Co., Ltd., Hangzhou 310051, China

* Correspondence: huang-yd@foxmail.com; Tel.: +86-15869172076

Abstract: Electroless nickel composite coatings have the potential for high-temperature tribological applications, and a combination of high wear resistance and low friction factor is one of the desirable solutions but still a tricky problem. The addition of self-lubricating WS₂ and hard Si₃N₄ nanoparticles to the Ni-P coatings is expected to obtain good high-temperature tribological performance. In this work, Ni-P-Si₃N₄-WS₂ composite coatings with various contents of WS₂ nanoparticles were prepared using electroless plating and subsequently annealed at 400 °C in an inert atmosphere. The tribological properties of the coatings were evaluated using a ball-on-disc wear instrument at operating temperatures from 25 to 600 °C. The microstructure, chemical composition, and surface morphology of the coatings were characterized by X-ray diffractometry (XRD), energy disperse spectroscopy (EDS), and scanning electron microscopy (SEM). Upon increasing the WS₂ dosage in the bath, the WS₂ content in the coating increased and the micro-hardness of the as-plated coating increased from 539 to 717 HV. After heat treatment, the coating underwent a crystallization process, and the hardness increased from 878 to 1094 HV. The main wear mechanism of the coating changed from adhesive wear in the as-plated state to abrasive wear in the annealed state. The annealed Ni-P-Si₃N₄-WS₂ coating with a WS₂ dosage of 2.5 g/L in the bath exhibited excellent mechanical properties, with a hardness of 10.9 GPa, a friction coefficient of ~0.51, and a wear rate of $8.4 \times 10^{-15} \text{ m}^3\text{N}^{-1}\cdot\text{m}^{-1}$ at room temperature, and maintained optimal performance at high temperatures. At operating temperatures of 200, 400, and 600 °C, the form of wear was adhesive wear for coatings with a WS₂ dosage <1.5 g/L and abrasive wear for coatings with a WS₂ dosage ≥ 1.5 g/L. The synergism of WS₂ and Si₃N₄ particles refined the grains of the Ni-P matrix in as-plated coatings and obviously reduced the friction coefficient of friction pairs in annealed coatings at all operating temperatures.

Keywords: composite coating; nanoparticles; nickel phosphorus alloy; electroless plating; friction; high temperature wear



Citation: Zheng, X.; Huang, Y.; Cai, C.; Huang, H.; Yang, F. High Temperature Tribological Behavior of Electroless Plating Ni-P-Si₃N₄-WS₂ Composite Coatings. *Coatings* **2023**, *13*, 723. <https://doi.org/10.3390/coatings13040723>

Academic Editors: Chi Ma, Esteban Broitman and Manuel António Peralta Evaristo

Received: 23 February 2023

Revised: 29 March 2023

Accepted: 31 March 2023

Published: 2 April 2023



Copyright: © 2023 by the authors. Licensee MDPI, Basel, Switzerland. This article is an open access article distributed under the terms and conditions of the Creative Commons Attribution (CC BY) license (<https://creativecommons.org/licenses/by/4.0/>).

1. Introduction

As a coating method, electroless plating has been widely used in electronics, automobiles, the chemical industry, aviation, and other industrial fields because of its simple processing conditions, uniform coating thickness, good wear, and corrosion resistance [1,2]. At the same time, electroless plating has good applicability. The coatings can be deposited on the surface of pretreated nonmetallic materials, such as spherical SiO₂ [3] or carbon nitride [4]. Ni-P electroless coatings were the first widely used electroless coatings due to their good wear resistance and corrosion resistance, which is related to their P content [5]. Furthermore, electroless nickel plating could be used on zirconia ceramic for hip replacement joints. However, the properties of traditional Ni-P electroless coatings cannot meet people's other needs in the technologically progressing world.

In recent decades, scholars have successfully developed two methods to obtain electroless composite coatings. One is the co-deposition of other metal cations with Ni ions in a bath, to achieve multielement electroless coatings, such as Ni-Cu-P [6], Ni-Mo-P [7], and Ni-W-P [8,9] coatings. The other is the incorporation of micro- or nanoscale particles to simple Ni-P coatings, such as hard particle SiC [10], B₄C [11], Al₂O₃ [12], Si₃N₄ [13,14], soft particle CeO₂ [15] and WS₂ [16] to enhance the wear resistance, corrosion resistance or self-lubricating properties of the coatings. In addition, the catalytic performance of electroless composite coatings, such as Ni-Co-P [17] and Ni-P-CuO [18] coatings, were also involved. To satisfy the increasingly severe demand for various tribological applications, two or more kinds of particles have been added into the bath to further improve the coatings' tribological performance, such as Ni-P-Al₂O₃-WS₂ [19], Ni-P-ZrO₂-CeO₂ [20], and Ni-B-W-SiC coatings [21]. These studies have explored the effect of different nanoparticles on the wear behavior of nickel phosphorus coatings at room temperature well. Additionally, it is helpful to establish a computational wear model of thick composite coatings. The computational simulation approach to tribological investigation has been well developed for the friction pairs served at room temperature, such as for artificial joint prosthesis [22–24], and exhibits obvious advantages in low cost, great efficiency and wide applicability compared to the traditional experimental testing.

However, there are still many applications that require the coatings to work at high temperatures. High temperature is a harsh condition for most friction applications, the oxidation and deformation of the coatings are remarkably larger than those of room temperature during wear process, and the generation rate, the removal rate of thin oxide layers and the corresponding effects are hardly simulated; therefore, experimental testing is still a realistic approach to the investigation of high temperature tribological properties of the coatings. Whenever friction components are operated at high temperatures or suffer a considerable rise in temperature due to a high-speed and heavy-load condition, traditional lubricating media such as liquid lubricants will decompose quickly and are no longer effective [25]. A good way to solve this problem is using solid lubricants [26], such as MoS₂, WS₂, graphite, or hexagonal boron nitride (hBN) [27], and many studies have been performed to improve the high-temperature wear resistance of the Ni-P based coatings. For example, Zhen Li et al. investigated the friction properties of a Ni-P-MoS₂ composite coating at 25 to 600 °C [28], and the best tribological properties of the composite coating were obtained at 400 °C. Sanming Du et al. found that a Ni-P-MoS₂-CaF₂ composite coating has a stable friction coefficient at 200 to 570 °C [29]. As two solid lubricants were combined into a composite material, they provided effective lubrication over a broad range of temperatures. However, the hardness of the coating was relatively low, possibly due to the two soft phases, and the coating had a high friction coefficient and high wear rate at room temperatures. Şeyma Ürdem et al. studied the wear behavior of the NiB-Al₂O₃ coating at high temperature [30]. The effects of Al₂O₃ addition and temperature on the tribological process of the coatings was explained. Due to the incorporation of Al₂O₃ hard particles, the coating has a hardness of 1260 HV but a high friction coefficient at 600 °C. Generally, electroless nickel composite coatings have the potential for high-temperature applications after incorporating specific nanoparticles [31].

In recent years, WS₂ has attracted more attention in tribological applications because it has similar self-lubrication properties comparable to MoS₂ and is resistant to oxidation up to approximately 450 °C (350 °C for MoS₂) [32], providing the potential to improve the high temperature properties of the Ni-P-TMS (Transition Metal Sulfide)-based composite coating. In this work, we introduced the hard nanoparticle Si₃N₄ and self-lubricating nanoparticle WS₂ to the Ni-P coating, avoiding a low hardness of composite coatings with two soft lubricants [29]. The effects of the co-addition of Si₃N₄ and WS₂ nanoparticles, heat treatment and service temperature on the tribological behavior of the Ni-P-Si₃N₄-WS₂ composite coatings were investigated. The synergetic effect between WS₂ and Si₃N₄ and the wear mechanism of the coatings were also discussed. The obtained results will provide

the basic data for the computational simulation of high-temperature wear properties of composite coatings.

2. Materials and Methods

2.1. Preparation of Composite Coatings

Q235A steel plates were used as the substrates, and the size was 20 mm × 25 mm × 2 mm. Both the Si₃N₄ and WS₂ nano-powders are commercially available (Bisili new materials Co., Ltd. SuZhou, China), with an average particle size of ~100 nm. Before deposition, the steel disks were ground using 1000-grade SiC abrasive paper. Then, the substrates were degreased in alkaline solution. After being rinsed with deionized water, they were activated in approximately 10% HCl solution. The components of the plating bath and the operating parameters used in the experiments are shown in Table 1. The Si₃N₄ dosage was fixed at 5.0 g/L based on the optimal value for the tribological performance of Ni-P-Si₃N₄ coatings. Figure 1 shows the specific process.

Table 1. Components of the electroless plating bath.

Components of the Bath	Dosage (g/L)
Nickel sulfate	25
Sodium hypophosphite	30
Sodium citrate	15
Sodium acetate	15
Glycine	5
Succinic acid	5
Stabilizer	Appropriate dosage
Si ₃ N ₄ powders	5.0
WS ₂ powders	0, 0.5, 1.0, 1.5, 2.0, 2.5

Operating conditions: bath temperature of (80 ± 2) °C; pH value of (4.4–4.8); plating duration of 2 h.

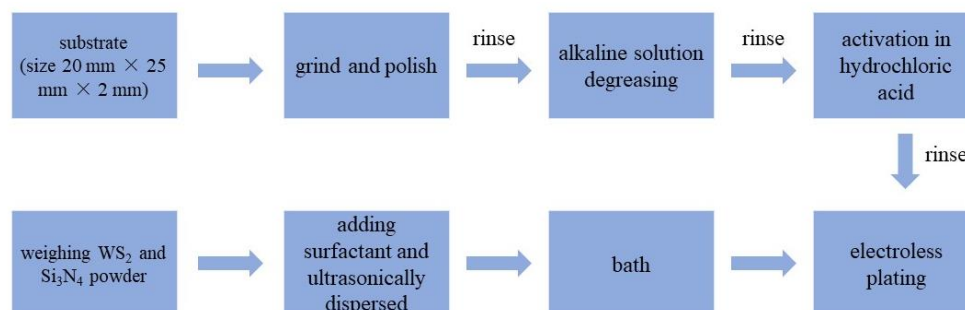


Figure 1. Preparation process of composite coatings.

The plating bath was prepared according to its formula. Then, the required mass of WS₂ and Si₃N₄ powders were weighed and ultrasonically dispersed in 20 mL of distilled water with an appropriate amount of surfactant for 15 min. After the pretreatment of the substrates was finished, the prepared suspension of nano-powders was added to the plating bath within 1 min at a uniform rate. Subsequently, the substrates were immersed in the bath for plating. Mechanical stirring was used with a fixed speed of 250 rpm, and the plating duration was 2 h. During the plating process, the pH value of the bath was adjusted with a dilute sulfuric acid solution (1 mol/L) every 20 min. Finally, six groups of samples with different WS₂ contents were prepared. For the purpose of comparison, a pure Ni-P coating and a Ni-P-WS₂ coating (WS₂ dosage = 2.5 g/L in bath) were also prepared.

For all the samples, a post-annealing process was conducted in an argon gas atmosphere with a temperature of 400 °C and a duration of 1 h.

2.2. Characterization and Wear Test

The phase structure of the samples was analyzed by an X-ray diffractometer (X'Pert PRO, Nalytical company of Almero, The Netherlands) in the diffraction angle range of

10°~80° with a scanning speed of 2°/min. The operating parameters of the X-ray tube were as follows: Cu target, K_{α} radiation (wavelength = 0.15406 nm), and working voltage of 40 kV, working current of 40 mA. The surface morphology of the samples was observed using a scanning electron microscope (Nova Nano 450, FEI company of Hillsboro, OR, USA) with an accelerating voltage of 15 kV. The chemical composition of the samples was analyzed using an energy dispersive spectrometer (QUANTAX EDS, BRUKER of Billerica, MA, USA) equipped with a scanning electron microscope, and an average of 5 measurements was used.

The hardness of the samples was measured using a Vickers hardness tester (HX-1000TM, Shanghai Lidun Instrument Testing Technology Co. LTD, Shanghai, China) with a load of 0.98 N and a holding time of 15 s. The thickness of the coating was measured by observing the sample's cross-section with a metallographic microscope (BX51M, OLYMPUS of Tokyo, Japan), and was reported at 17.0, 16.6, 15.8, 15.5, 14.9, 14.5 μm with an increased WS_2 dosage. Ni-P and Ni-P- WS_2 coatings had thicknesses of 22.0 and 12 μm . The tribological property of the coating was tested using a ball-on-disc tribotester (HT-600, Lanzhou Zhongkekaihua company of Lanzhou, China). The sample was used as the friction disc, and a polished silicon nitride ceramic ball (diameter in 3 mm, hardness in HV1200) was used as the counterpart. The normal load was 1.96 N and the test duration was 15 min. The test was carried out at room temperature (25 °C), 200, 400 and 600 °C. Each tribological test was repeated 3 times. After the wear test, the cross-sectional profiles of the wear track were measured using a surface profiler (Dektak 150 Surface Profiler, Veeco company of New York, New York, NY, USA) at 5 random positions, then the wear volume was calculated by integrating the worn profile along the whole wear circle, and the average was used as the wear volume of the sample. The specific wear rate was obtained by the formula: Wear rate = Wear volume/(Normal load \times Sliding distance).

3. Results and Discussions

3.1. Microstructure of the Coatings

Table 2 shows the chemical composition of the coatings, including the elements of Ni, P, Si, N, W, S, and a certain amount of O. Because the peak position (related to X-ray photon energy) of the S element is relatively close to that of the N element for EDS detection, a resulting content error of S and N element occurred to some extent. Therefore, the contents of WS_2 and Si_3N_4 in the coatings were subject to the W and Si elements, respectively. It can be seen from Table 2 that, as WS_2 dosage in the bath increased, W content in the coatings increased and Si content decreased gradually, indicating an increased WS_2 and decreased Si_3N_4 content in the coating. However, the content of WS_2 tended towards a constant in the WS_2 dosage range of 2.0–2.5 g/L. According to these data, the Ni/P mass ratio ($\omega_{\text{Ni}}/\omega_{\text{P}}$) of Ni-P- Si_3N_4 - WS_2 coatings was calculated and ranges from 9.33 to 10.73, larger than those of single Ni-P ($\omega_{\text{Ni}}/\omega_{\text{P}} = 8.87$) and Ni-P- WS_2 coatings ($\omega_{\text{Ni}}/\omega_{\text{P}} = 8.05$), indicating a lower P content of Ni-P matrix in Ni-P- Si_3N_4 - WS_2 coatings. Compared with the other samples, the Ni-P- WS_2 coating presents a higher content of O, which is probably due to the heavy adsorption of oxygen on the surface of the coating.

Table 2. Chemical composition of Ni-P, Ni-P- WS_2 and Ni-P- Si_3N_4 - WS_2 coatings (mass fraction).

Element	Ni-P	Ni-P- WS_2	Ni-P- Si_3N_4 - WS_2					
			0 g/L	0.5 g/L	1.0 g/L	1.5 g/L	2.0 g/L	2.5 g/L
Ni	89.3 \pm 2.2	81.0 \pm 2.1	71.8 \pm 1.8	75.1 \pm 1.9	76.8 \pm 1.9	75.9 \pm 1.9	75.3 \pm 1.9	75.9 \pm 1.9
P	10.1 \pm 0.3	10.0 \pm 0.3	7.7 \pm 0.3	7.0 \pm 0.3	7.4 \pm 0.3	7.3 \pm 0.3	7.1 \pm 0.3	7.1 \pm 0.3
Si	-	-	12.4 \pm 0.3	8.8 \pm 0.3	8.2 \pm 0.3	8.0 \pm 0.3	7.6 \pm 0.3	7.4 \pm 0.3
N	-	-	7.1 \pm 1.3	7.5 \pm 1.4	5.9 \pm 0.9	6.2 \pm 1.0	6.1 \pm 0.9	5.6 \pm 0.8
S	-	1.0 \pm 0.1	-	0.1 \pm 0.1	0.1 \pm 0.1	0.3 \pm 0.2	0.4 \pm 0.2	0.5 \pm 0.2
W	-	3.2 \pm 0.1	-	0.4 \pm 0.1	0.6 \pm 0.1	1.3 \pm 0.1	2.5 \pm 0.1	2.5 \pm 0.1
O	0.6 \pm 0.2	4.8 \pm 0.2	1.0 \pm 0.2	0.9 \pm 0.2	1.0 \pm 0.2	1.0 \pm 0.2	1.0 \pm 0.2	0.8 \pm 0.2

Figure 2 shows the SEM morphology of the as-plated samples recorded by a secondary electrons (SE) detector and a back-scattered electrons (BSE) detector. In Figure 2a, the surface of the Ni-P coating was relatively flat with distinguishable pinholes (corresponding to the black spots), and the size of the lumps was large (2–15 μm). However, the morphology of Ni-P-Si₃N₄-WS₂ coatings (Figure 2b–d) consisted of many fine lumps (1–2 μm in size) and black dots. According to the results from the EDS analysis, the black dots in Figure 2b–d correspond to Si₃N₄ particles. Furthermore, WS₂ particles in the Ni-P-Si₃N₄-WS₂ coatings are not easy to distinguish, which is probably due to their low content. Figure 1e shows the backscattered electron (BSE) image corresponding to Figure 2d, in which the Si₃N₄ particles (black part) were evenly distributed, while the bright white part (marked with white circles) corresponds to WS₂ particles. As for the Ni-P-WS₂ coating, its morphology appears different from that of the other coatings; many loosely aggregated grains lie on the surface of the Ni-P matrix, consequently promoting the heavy adsorption of oxygen on the coating's surface. The reason for this phenomenon can be attributed to the change in the growth environment of the Ni-P matrix due to the addition of WS₂ particles. WS₂ particles were not only embedded in the Ni-P matrix directly, but also well-coated with Ni-P alloy and then deposited on the coating's surface. Most notably, after Si₃N₄ nano-powders were added to the bath, the lump size of the Ni-P matrix remarkably decreased, suggesting a considerable grain refinement in the microstructure. A possible mechanism is that the Si₃N₄ particles attached or embedded on the surface significantly blocked the growth of the Ni-P lumps [14].

Figure 3a shows the XRD patterns of the as-plated coatings. There was a diffuse peak at about 45° for each sample, very similar to those of typical amorphous Ni-P alloys with a phosphorus mass fraction higher than 8% (i.e., $\omega_{\text{Ni}}/\omega_{\text{P}} = 11.5$) [33]. The peak at 2θ of 14.32° corresponded to the WS₂ (002) plane, and the rest were the peaks of the (101), (110), (200), (201), (102), and (210) planes of Si₃N₄. With the increase in WS₂ dosage, Si₃N₄ and WS₂ phases in the coatings maintained a crystalline structure, and the Ni-P matrix remained amorphous. The formation of an amorphous Ni-P matrix is easily understood, because each sample in this work presented a $\omega_{\text{Ni}}/\omega_{\text{P}}$ value less than 11.5; for example, the phosphorus content of the Ni-P matrix was higher than 8%. After annealing at 400 °C, Ni₃P and Ni phases appeared in the samples (see Figure 3b), indicating that the crystallization reaction occurred in the amorphous Ni-P matrix [34,35], while the peaks of WS₂ and Si₃N₄ still existed, indicating that the two kinds of nanoparticles had good thermal stability without obvious structural transformation or decomposition [36]. The other Ni-P-Si₃N₄-WS₂ coatings exhibited a similar crystallization reaction, as well.

3.2. Mechanical Properties

Figure 4 shows the dependence between the micro-hardness of the coatings and the WS₂ dosage in the bath before and after heat treatment. At the as-plated state, the hardness of the Ni-P coating was 4.6 GPa, while the Ni-P-WS₂ coating demonstrated a relatively lower hardness (3.6 GPa), the possible reason for which can be attributed to a loose morphology of the Ni-P-WS₂ coating (see Figure 2f) and the low strength of WS₂ particles, causing the coating's strength to decrease. When Si₃N₄ and WS₂ particles were simultaneously added to the bath, the hardness of the Ni-P-Si₃N₄-WS₂ coating was remarkably higher than that of the Ni-P-WS₂ coating, which is mainly due to the high strength of Si₃N₄ particles. Furthermore, with the increase in WS₂ dosage, the agglomeration level of WS₂ particles on the coating's surface decreased, and the microstructure of the coating became finer. Therefore, the synergism of Si₃N₄ and WS₂ powders made the coating denser and the microstructure finer, so the hardness of the coating showed an upward trend and reached the highest value of 7.2 GPa at a WS₂ dosage of 2.5 g/L. The fine-grain strengthening effect played a main role in the progressive increase in the coating's hardness.

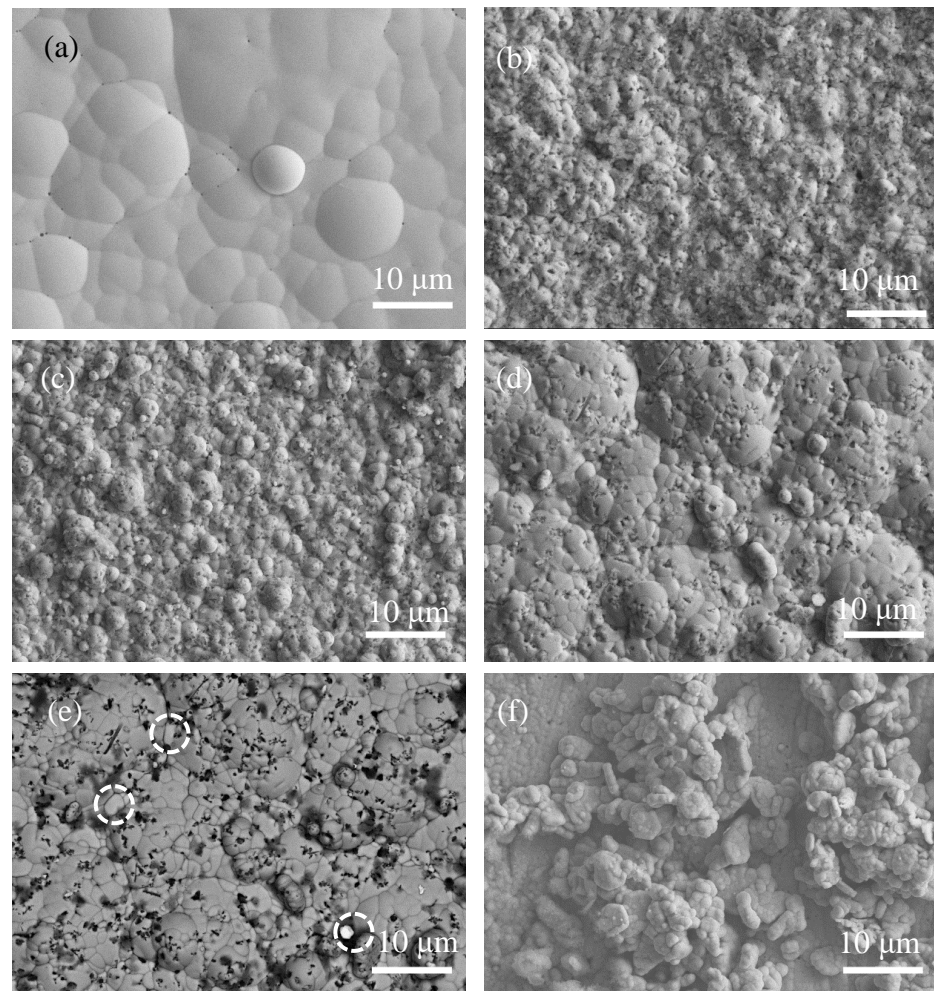


Figure 2. Surface morphologies of as-plated coatings: (a) Ni-P (SE); (b) Ni-P-Si₃N₄ (SE); (c) Ni-P-Si₃N₄-WS₂, 1.5 g/L (SE); (d) Ni-P-Si₃N₄-WS₂, 2.5 g/L (SE); (e) Ni-P-Si₃N₄-WS₂, 2.5 g/L (BSE), WS₂ particles in white circles; (f) Ni-P-WS₂, 2.5 g/L (SE).

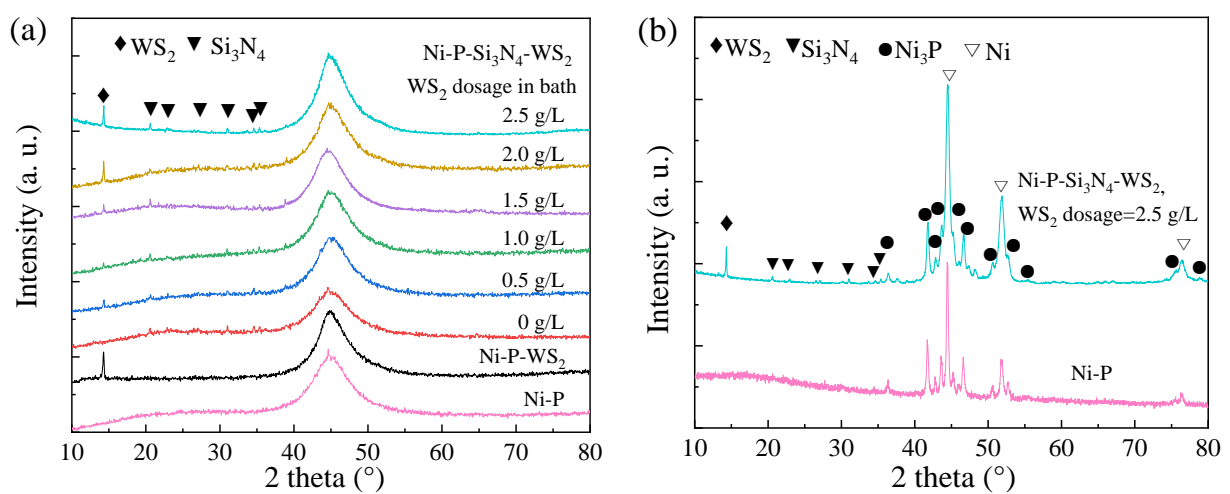


Figure 3. XRD patterns of Ni-P based coatings with various WS₂ dosages in bath: (a) as-plated; (b) annealed.

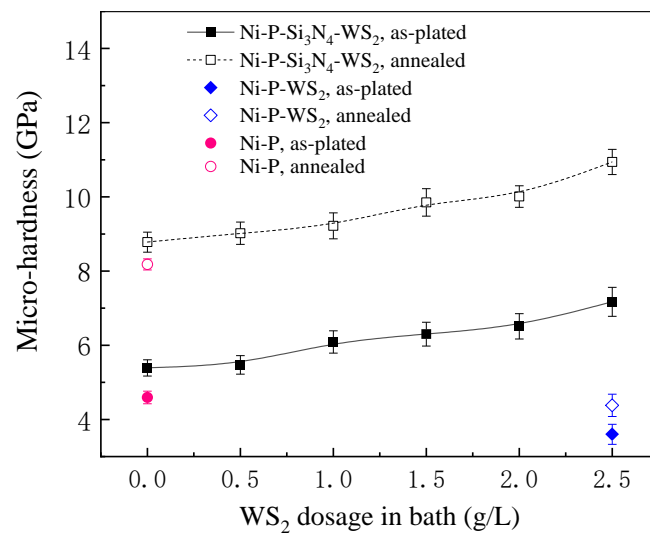


Figure 4. Dependence of the hardness of Ni-based coatings with WS₂ dosage in bath.

After annealing, the hardness of each coating greatly improved, and the Ni-P-Si₃N₄-WS₂ coating with a WS₂ dosage of 2.5 g/L exhibited the highest hardness at 10.9 GPa. This can be attributed to the crystal transformation of the amorphous Ni-P matrix during annealing; a large number of Ni₃P particles were precipitated and uniformly dispersed in the Ni solid solution, remarkably hindering the dislocation movement and inhibiting plastic deformation. At the same time, WS₂ and Si₃N₄ particles embedded in the coating played the role of pinning during the transformation of the amorphous Ni-P matrix, which made the grain size smaller after crystallization and thereby provoked a more prominent effect of fine-grain strengthening.

Figure 5a shows the mean friction coefficient (operated at room temperature) of the coatings before and after heat treatment, and both cases demonstrate a downward trend with increasing WS₂ dosage. In the as-plated state, the fact that the friction coefficient of the Ni-P-Si₃N₄-WS₂ composite coating is always lower than that of the Ni-P coating (=1.17) indicates that the addition of Si₃N₄ and WS₂ nano-powders is conducive to reducing the coating's friction coefficient, and thus effectively decreases the shear force applied on the coating in the wear process. Because the surface of the pure Ni-P coating is relatively flat and the normal load is relatively large (the load produces a theoretically calculated Hertz contact stress of ~1.52 GPa with the relevant parameters of an elastic modulus of Si₃N₄ ~385 GPa, an elastic modulus of Ni-P alloy of ~200 GPa, and Poisson's ratio of 0.3 for both), the actual contact area of the tribo-pair is large. After Si₃N₄ particles were added to the Ni-P matrix, the Si₃N₄ phase of high hardness played a supporting role in the coating and reduces the actual contact area, so the friction coefficient decreased [37]. After WS₂ particles were added, WS₂ particles played the role of self-lubrication when in contact with the friction ball, and the friction coefficient of the coating decreased significantly with the increase in WS₂ content. After annealing, the friction coefficient of Ni-P-Si₃N₄-WS₂ coating was significantly lower than that of the as-plated coating; the main reason is that the precipitation of the Ni₃P phase improves the coating's hardness and reduces the actual contact area of the tribo-pair. Notably, the friction coefficient of the Ni-P-Si₃N₄-WS₂ coating decreased rapidly when the WS₂ dosage exceeded 1.0 g/L and reached the minimum value of 0.51, slightly higher than the friction coefficient (=0.43) of the Ni-P-WS₂ coating at a WS₂ dosage of 2.5 g/L, suggesting that the addition of Si₃N₄ particles at a dosage of 5.0 g/L to the Ni-P-WS₂ coating only slightly increased the coating's friction coefficient. Therefore, the friction-reduction action of WS₂ particles and the synergism of WS₂ and Si₃N₄ particles are more pronounced.

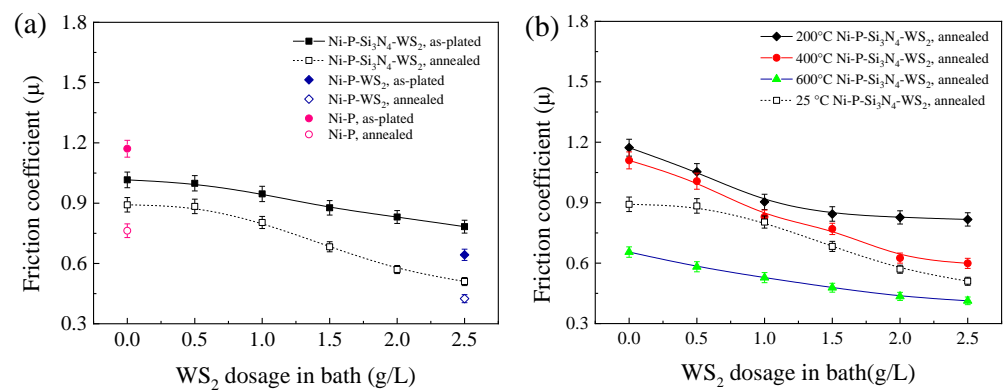


Figure 5. Dependence of the friction coefficient of Ni-based coatings on WS₂ dosage in bath: (a) at room temperature and (b) at 200, 400, and 600 °C (the data at R.T. are also included for comparison).

Figure 5b shows the mean friction coefficient of the annealed coatings at operating temperatures of 200, 400, and 600 °C. The downward trend is consistent with that of the coating operating at room temperature, and the friction coefficient reached its minimum value at a WS₂ dosage of 2.5 g/L. It has been proved that the WS₂ particles still maintain lubrication in the friction process at high temperatures. The friction coefficient of the Ni-P-Si₃N₄-WS₂ coating at 200 and 400 °C is higher than at 25 °C. The main reason is the decreased hardness of the coating with an increased operating temperature, and the increase in the actual contact area between the ceramic ball and the coating, which increases the friction coefficient. It is worth noting that the friction coefficient of the coating reaches a minimum value at 600 °C. The main reason is that the coating becomes softer at 600 °C, leading to a lower shear strength, and a low-stress abrasive wear was found in the friction pairs [30]. In addition, a low friction coefficient of the coatings is also related to the lubrication effect of WS₂ nanoparticles at various operating temperatures.

3.3. Wear Behavior at Room Temperature

Figure 6 shows the SEM surface morphology of the as-plated coatings after wear tests were carried out at room temperature. In Figure 6a, the scratch contour produced by the plowing of a ceramic ball is clear on the surface of the Ni-P coating. There are some peeling pits of wear debris in the wear mark area, and the furrow and adhesion effects of the sample are obvious, suggesting a typical adhesive wear characteristic. Compared with the Ni-P coating, the scratches on the Ni-P-WS₂ coating's surface (Figure 6f) are relatively finer, the wear mark is much wider, and more debris is accumulated. In Figure 6b–e, the wear debris is paved on the coating's surface under the rolling of the ceramic ball (spalling occurs in local areas due to poor adhesion of the debris to the coating's surface), and almost no coarse scratches are observed. The form of wear is mainly adhesive wear, with a polishing effect of nano-particles, which is the result of the synergetic action of WS₂ and Si₃N₄ nanoparticles. When in contact with the counterpart ball, the particles that were loosely bonded to the coating's surface first fell off. After the WS₂ particles peeled off, they spread on the coating's surface to form a lubricating layer, while Si₃N₄ played the role of abrasive polishing as a hard phase. The synergetic action of the two phases enhanced the friction performance of the coating [38]. Table 3 shows the chemical composition of the area of the wear mark (labeled with a white box in Figure 6). Compared with the original surface of the coating, the oxygen content in the wear mark area increased significantly, indicating that there was a lot of Ni oxide at the wear mark after wear tests, due to the tribo-chemistry effect in an ambient atmosphere.

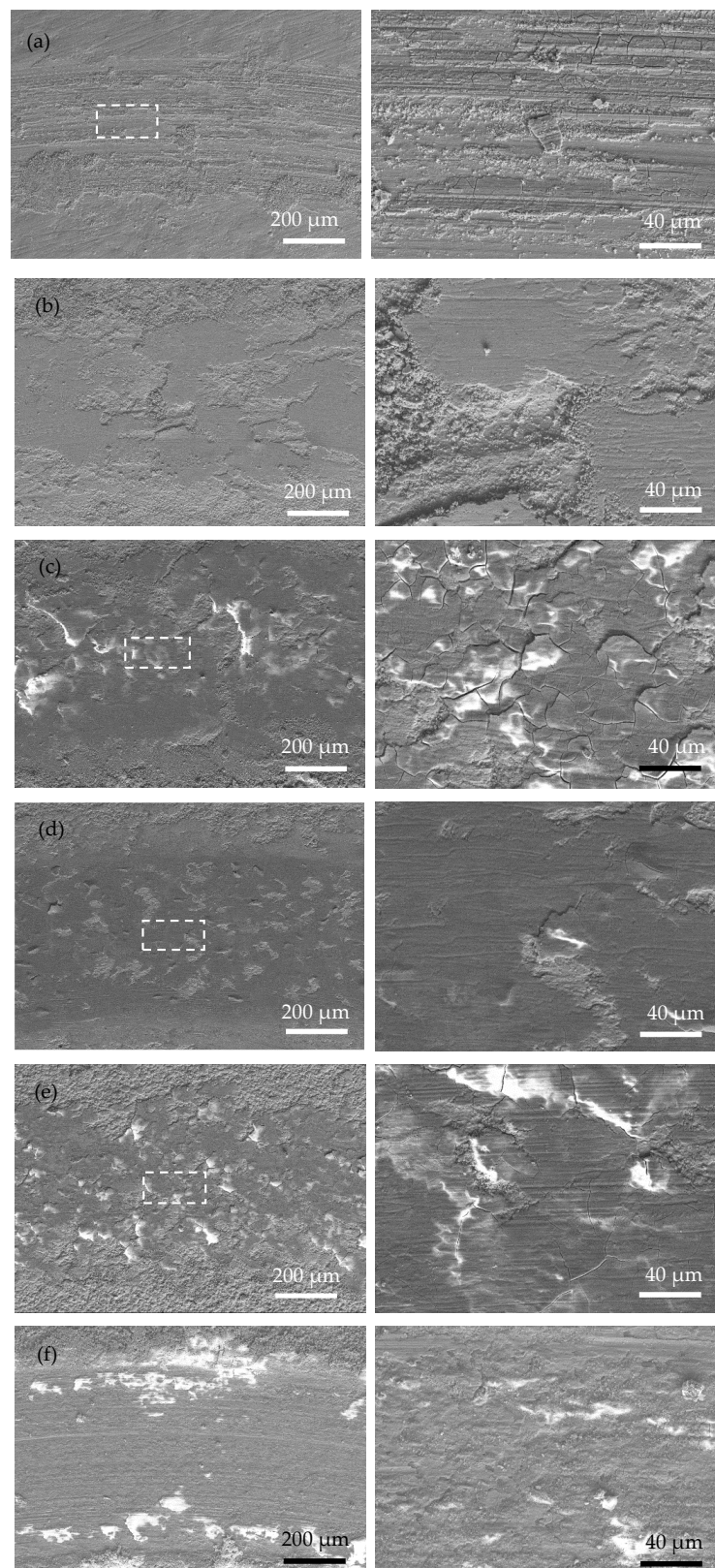
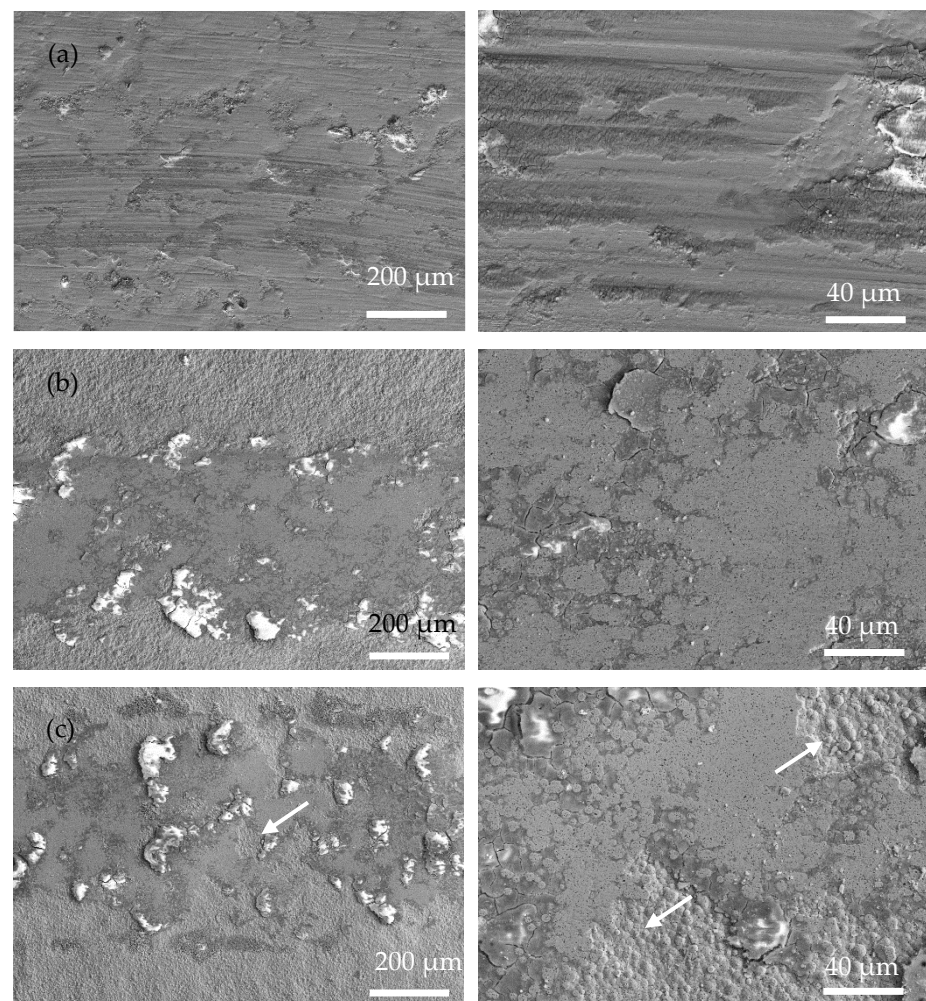


Figure 6. Surface morphology of the wear scar of the as-plated coatings at low magnification (left) and high magnification (right), the dotted frame means the scanning area of Table 3: (a) Ni-P; (b) Ni-P-Si₃N₄; (c) Ni-P-Si₃N₄-WS₂, 0.5 g/L; (d) Ni-P-Si₃N₄-WS₂, 1.5 g/L; (e) Ni-P-Si₃N₄-WS₂, 2.5 g/L; (f) Ni-P-WS₂.

Table 3. Chemical composition of wear mark (mass fraction).

Element	Ni-P	Ni-P-Si ₃ N ₄ -WS ₂		
		0.5 g/L	1.5 g/L	2.5 g/L
Ni	77.3	70.1	50.3	54.6
P	8.0	5.8	4.4	4.2
O	12.7	16.8	33.3	32.6
Si	0.5	3.6	8.5	5.3
N	0.6	1.5	2.0	1.4
S	-	0.1	0.1	0.2
W	-	0.7	1.2	1.5
Fe	0.9	1.4	0.2	0.2

Figure 7 shows the SEM wear morphology of the annealed coatings. Compared with that of the as-plated coatings, the area of the wear mark is smoother, with fewer cracks and plowing marks. The wear mechanism is mainly an abrasive polishing effect. Due to the obvious increase in the hardness of the annealed coating, the actual contact area between the coating and the ceramic ball became smaller during the friction process. Therefore, the depth and width of the wear mark are smaller than those of the as-plated coating, suggesting a better anti-wear property of the annealed coating. In addition, a large number of original surfaces appear in the wear mark area (marked with white arrows in Figure 7c–e), further proving that relatively slight wear occurred in the annealed coating.

**Figure 7.** Cont.

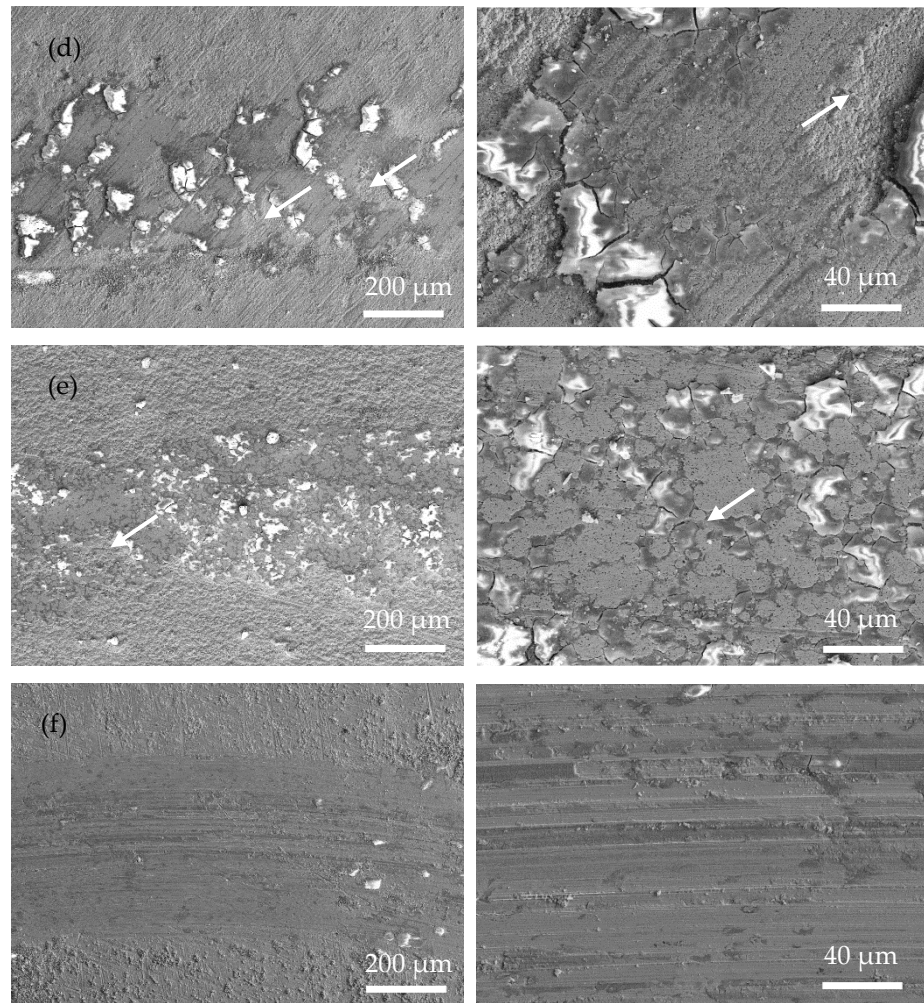


Figure 7. Surface morphology of the wear scar of the as-plated coatings at low magnification (left) and high magnification (right) (white arrow means original surface): (a) Ni-P; (b) Ni-P-Si₃N₄; (c) Ni-P-Si₃N₄-WS₂, 0.5 g/L; (d) Ni-P-Si₃N₄-WS₂, 1.5 g/L; (e) Ni-P-Si₃N₄-WS₂, 2.5 g/L; and (f) Ni-P-WS₂.

3.4. Wear Behavior at High Temperature

Figure 8 shows SEM images of the wear tracks of the coatings at operating temperatures of 200, 400, and 600 °C. Obviously, the width of the wear track of the coating is closely related to the operating temperature. Due to the rise in operating temperature, the softening of the substrate and coating led to a decrease in hardness and then an increased contact area of the friction pairs. Severe adhesive wear of the Ni-P coating occurred at high temperatures, and at 600 °C there were pits at the wear track and the form of wear was gluey wear. As a result, the coating exhibits a wider wear track at higher temperatures. In Figure 8, Ni-P and Ni-P-Si₃N₄-WS₂ (0.5 g/L) coatings show a wider wear track than Ni-P-Si₃N₄-WS₂ (1.5 g/L) or Ni-P-Si₃N₄-WS₂ (2.5 g/L) coatings. Meanwhile, it can be seen from Figure 8a,b that there are some flaking marks on the wear area, and the wear form was mainly adhesive wear. Under the pressure of a ceramic ball, the stress at the contact peak reached the coating's yield limit and produced plastic deformation. Then, the adhesion node was sheared or even peeled off during the wear process. As the temperature increased, this adhesion effect was further intensified, and the coating showed tracks of being crushed at 400 °C. When the operating temperature rose to 600 °C, there were some micro-cracks in the abrasion marks, which were caused by the cyclic stress impact of adhesive friction. In Figure 8c,d, the overall scratch width shows a decreasing trend. Additionally, there are fine scratches on the wear marks, and the form of wear was mainly abrasive wear with a polishing effect of nanoparticles, which is the result of the interaction between WS₂

and Si_3N_4 nanoparticles. At the initial contact stage of friction pairs, the loosely bonded particles on the surface of the coating first fell off, and the spalling WS_2 particles spread on the surface of the coating to form a lubrication layer, and Si_3N_4 , as a hard phase, played the role of abrasive polishing. At the same time, the increase in temperature made the coating more prone to oxidation reaction, and the spalling oxides, together with Si_3N_4 and WS_2 nanoparticles, formed an intermediate friction layer in the process of wear. These tiny third phases act as abrasive polish, making the scratches smooth. As can be seen from Figure 9c,d, the two Ni-P- Si_3N_4 - WS_2 coatings maintained good wear resistance at 200 and 400 °C and can protect the matrix at 600 °C.

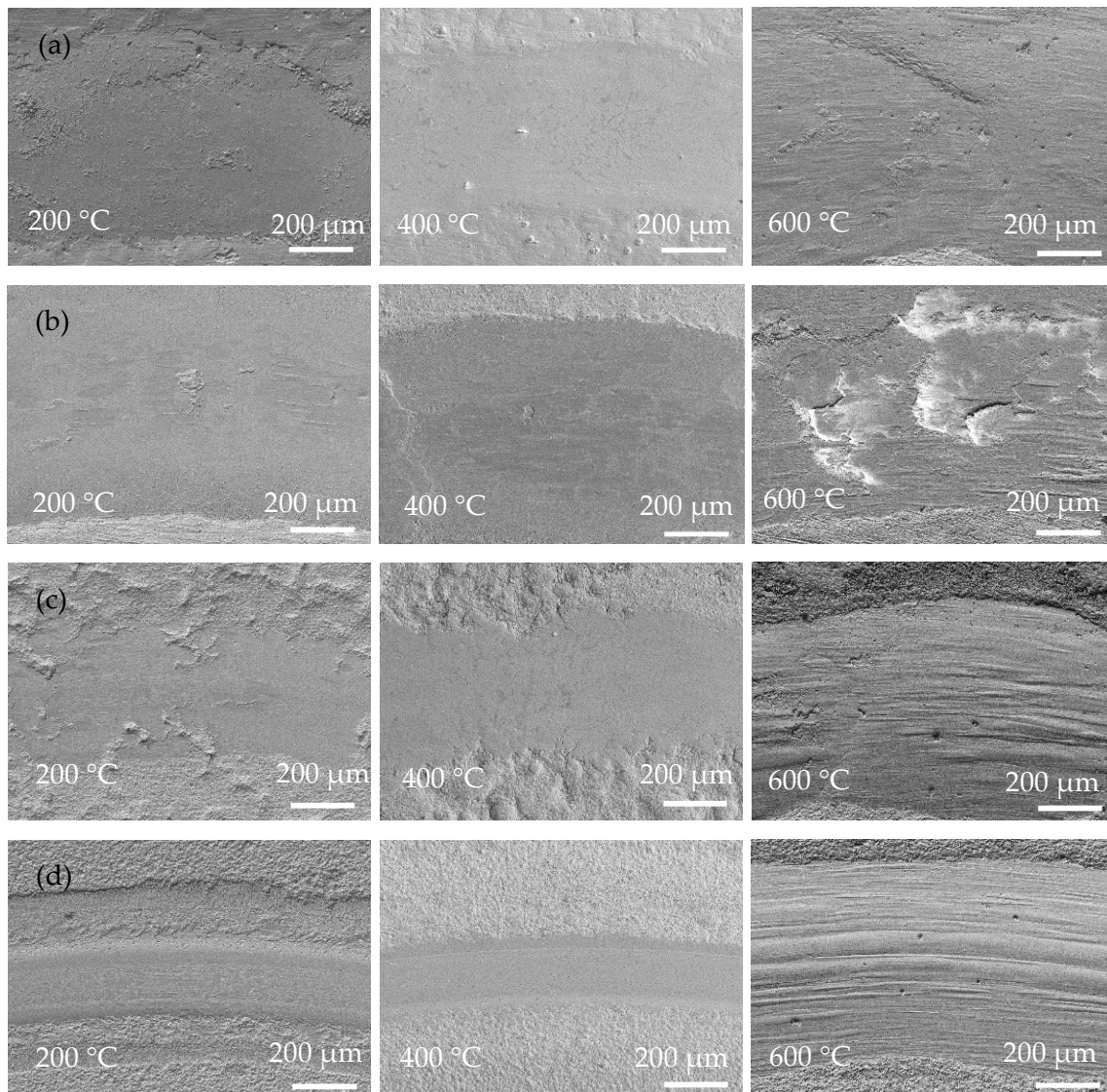


Figure 8. Low-magnification surface morphologies of wear scar of coatings operated at 200, 400, and 600 °C: (a) Ni-P; (b) Ni-P- Si_3N_4 - WS_2 , 0.5 g/L; (c) Ni-P- Si_3N_4 - WS_2 , 1.5 g/L; (d) Ni-P- Si_3N_4 - WS_2 , 2.5 g/L.

3.5. Wear Rate of the Coatings

Figure 10a shows the wear rates of the coatings before and after heat treatment at room temperature. Both presented a decreasing trend with the increase in WS_2 dosage. In the as-plated state, the wear rate of the coating with a WS_2 dosage of 2.5 g/L was only 19.8% of that of the pure Ni-P coating and 28.6% of that of the Ni-P- Si_3N_4 coating. As a self-lubricating particle, WS_2 has good anti-friction properties. In the friction process,

a lubricating layer is formed to rub with the friction pair, slowing down the wear of the alloy matrix [39]. In addition, with the increase in the WS₂ dosage in a bath, the grains of the coating become fine and dense, which improves the strength and improves the wear resistance. After annealing, the wear rate of the coating was only (1/5–1/8) of that in the as-plated state, suggesting a significantly improved wear resistance of the coatings, which can be attributed mainly to an obviously increased hardness of the coatings due to the precipitation of the Ni₃P phase after heat treatment.

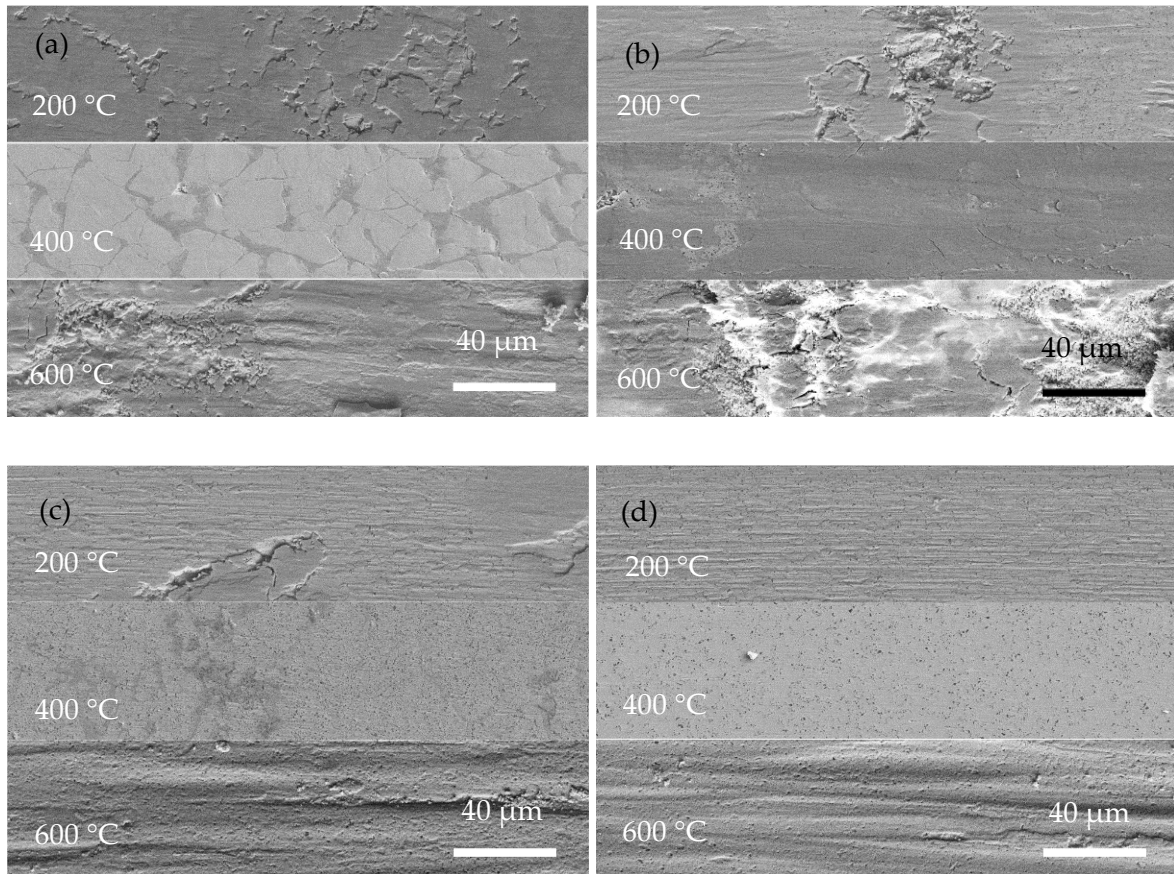


Figure 9. High-magnification surface morphologies of wear scar of coatings operated at 200 °C, 400 °C, and 600 °C: (a) Ni-P; (b) Ni-P-Si₃N₄-WS₂, 0.5 g/L; (c) Ni-P-Si₃N₄-WS₂, 1.5 g/L; (d) Ni-P-Si₃N₄-WS₂, 2.5 g/L.

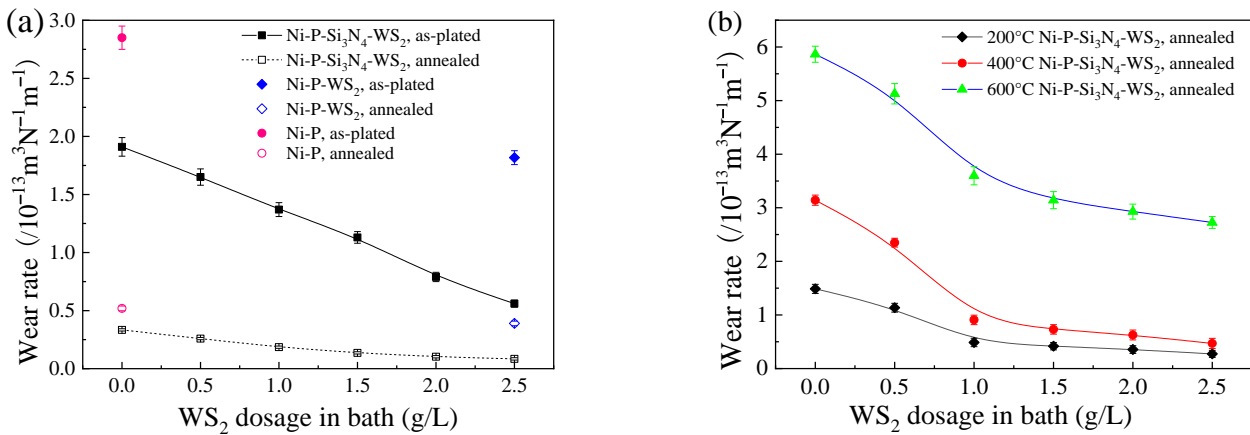


Figure 10. Wear rate of Ni-based coatings with WS₂ dosage in bath at various operating temperatures: (a) room temperature; (b) 200, 400, and 600 °C.

Figure 10b shows the wear rates of the coatings at operating temperatures of 200, 400, and 600 °C. It can be seen that the wear rate of the coating decreased monotonically with the increase in WS₂ dosage in a bath at each operating temperature, clearly indicating that the addition of WS₂ can effectively improve the wear resistance of the Ni-P-Si₃N₄ coating and that the anti-friction action of WS₂ is similar to the results from the literature [32]. These results can be attributed to the changes in the coating's hardness and wear mechanism of the friction pair. When the WS₂ dosage was less than 1.5 g/L, the form of wear was mainly adhesive wear. The contact area between the ceramic ball and the coating was large due to the relatively low hardness of the coating, and the wear rate was high. When WS₂ dosage reached a certain amount, the form of wear of the coating changed to abrasive wear, and the coating had a high hardness, which made the contact area of the friction pair small. In the friction process, Si₃N₄ and WS₂ nanoparticles were removed together with Ni particles and Ni oxide as the third phase, which improved the tribological properties of the coating. The wear rate at 600 °C reached the highest value, which was an order of magnitude higher than that of room temperature because the influence of temperature on wear is decisive. A high temperature will rapidly reduce the hardness of the coating and increase the contact area of the friction pair, and an oxidation wear reaction will easily occur in this condition.

As for the coatings tested at room temperature, based on the above results, the annealing process and the synergism of WS₂ and Si₃N₄ particles play an important role in the change in the main mechanism of wear and the enhancement of wear resistance of the coatings with increased WS₂ dosage. In the as-plated state, the hardness of the coating was obviously lower than that of the counterpart ball, the composite coating was prone to produce large plastic deformation, and the formed adhesion node on the counterpart ball underwent shear and fatigue and finally fell off to form wear debris. The synergism of WS₂ and Si₃N₄ particles contributed slightly to the reduction in the friction coefficient of the coating, and the as-plated coatings presented a wear mechanism dominated by adhesive wear. After annealing, the coating's hardness increased significantly, indicating a smaller plastic deformation under the same testing condition. The counterpart ball could only slightly plow the coating's surface and smooth the rough bumps, while the silicon nitride particles falling off the coating's surface acted as the polishing medium, and the rolling of these particles on the coating's surface could reduce the friction coefficient of the friction pair. Meanwhile, WS₂ particles further reduced the friction coefficient of the friction pair due to the low shear strength of the WS₂ phase. Consequently, the Ni-P-Si₃N₄-WS₂ coating with a WS₂ dosage of 2.5 g/L exhibited an excellent tribological property. The main wear mechanism of the annealed coatings was abrasive wear.

The enhancement of the tribological property of Ni-P-Si₃N₄-WS₂ coatings at high temperatures due to the addition of WS₂ nanoparticles to Ni-P-Si₃N₄ coatings was also confirmed. The WS₂ nanoparticles can still play a lubricating role at 600 °C, and the two nanoparticles formed the third term with the mixture of Ni metal and Ni oxide abrasive chips, which played the role of plowing and polishing on the coating, and the form of wear of the coating changed from adhesive wear to abrasive wear.

4. Conclusions

The WS₂ content in Ni-P-Si₃N₄-WS₂ coatings increased with an increase in WS₂ dosage in the bath. The synergism of WS₂ and Si₃N₄ particles refined the grains of the Ni-P matrix and obviously enhanced the coating's hardness. After annealing, the Ni-P-Si₃N₄-WS₂ coating underwent a crystallization reaction and its hardness was greatly improved. With increasing WS₂ dosage in the bath, the friction coefficient and wear rate of Ni-P-Si₃N₄-WS₂ coatings decreased monotonously at all operating temperatures. At room temperature, the main mechanism of wear of the coatings changed from adhesive wear in the as-plated state to abrasive wear in the annealed state. At operating temperatures of 200, 400, and 600 °C, the form of wear was adhesive wear for the coatings with a WS₂ dosage <1.5 g/L and abrasive wear for the coatings with a WS₂ dosage ≥1.5 g/L. It can be concluded that there was a strong synergism of WS₂ and Si₃N₄ particles in reducing

the friction coefficient of the friction pair in the annealed coatings. The annealed Ni-P-Si₃N₄-WS₂ coating with a WS₂ dosage of 2.5 g/L in the bath exhibited excellent mechanical properties, with a hardness of 10.9 GPa, a friction coefficient of ~0.51, and a wear rate of $8.4 \times 10^{-15} \text{ m}^3\text{N}^{-1}\cdot\text{m}^{-1}$ (when used at room temperature), and maintained an optimal performance at high temperatures.

Author Contributions: Conceptualization, X.Z. and Y.H.; methodology, X.Z.; software, Y.H.; validation, X.Z., Y.H. and C.C.; formal analysis, X.Z. and Y.H.; investigation, H.H.; resources, F.Y.; data curation, X.Z.; writing—original draft preparation, Y.H.; writing—review and editing, X.Z.; visualization, Y.H.; supervision, X.Z.; project administration, F.Y.; funding acquisition, X.Z. All authors have read and agreed to the published version of the manuscript.

Funding: This work was financially supported by the Zhejiang Provincial Key R&D Program (No. 2019C01088) and Enterprises Cooperative Project (No. KYY-HX-20220850).

Institutional Review Board Statement: Not applicable.

Informed Consent Statement: Not applicable.

Data Availability Statement: The data presented in this study are available on request from the corresponding author.

Conflicts of Interest: The authors declare no conflict of interest.

References

1. Sudagar, J.; Lian, J.; Sha, W. Electroless nickel, alloy, composite and nanocoatings—A critical review. *J. Alloys Compd.* **2013**, *571*, 183–204. [[CrossRef](#)]
2. Vitry, V.; Hastir, J.; Mégret, A.; Yazdani, S.; Yunacti, M.; Bonin, L. Recent advances in electroless nickel-boron coatings. *Surf. Coat. Technol.* **2022**, *429*, 127937. [[CrossRef](#)]
3. Zeng, L.; Wang, C.; Li, Y.; Hu, T. Synthesis of core-shell Ti@Ni-P spherical powder by Ni electroless plating. *Micron* **2021**, *143*, 103027. [[CrossRef](#)] [[PubMed](#)]
4. Wang, Y.; Li, Y.; Cao, S.; Yu, J. Ni-P cluster modified carbon nitride toward efficient photocatalytic hydrogen production. *Chin. J. Catal.* **2019**, *40*, 867–874. [[CrossRef](#)]
5. Salicio-Paz, A.; Ugarte, I.; Sort, J.; Pellicer, E.; García-Lecina, E. Full Optimization of an Electroless Nickel Solution: Boosting the Performance of Low-Phosphorous Coatings. *Materials* **2021**, *14*, 1501. [[CrossRef](#)]
6. Chen, J.; Zhao, G.; Matsuda, K.; Zou, Y. Microstructure evolution and corrosion resistance of Ni–Cu–P amorphous coating during crystallization process. *Appl. Surf. Sci.* **2019**, *484*, 835–844. [[CrossRef](#)]
7. Li, J.; Sun, C.; Roostaei, M.; Mahmoudi, M.; Fattahpour, V.; Zeng, H.; Luo, J.-L. Characterization and corrosion behavior of electroless Ni-Mo-P/Ni-P composite coating in CO₂/H₂S/Cl⁻ brine: Effects of Mo addition and heat treatment. *Surf. Coat. Technol.* **2020**, *403*, 126416. [[CrossRef](#)]
8. Liu, B.; Zhang, Q.; Li, Y.; Yang, Y.; Zhang, T.; Wang, Y.; Shao, Y.; Sun, H.; Wang, Z.; Wang, F. Optimization of the Corrosion Resistance of Electroless Ni–W–P Coatings on Magnesium Alloys by the Response Surface Methodology. *Coatings* **2021**, *11*, 18. [[CrossRef](#)]
9. Kundu, S.; Das, S.K.; Sahoo, P. Friction and wear behavior of electroless Ni-P-W coating exposed to elevated temperature. *Surf. Interfaces* **2019**, *14*, 192–207. [[CrossRef](#)]
10. Ghavidel, N.; Allahkaram, S.R.; Naderi, R.; Barzegar, M.; Bakhshandeh, H. Corrosion and wear behavior of an electroless Ni-P/nano-SiC coating on AZ31 Mg alloy obtained through environmentally-friendly conversion coating. *Surf. Coat. Technol.* **2020**, *382*, 125156. [[CrossRef](#)]
11. Ebrahimian-Hosseinabadi, M.; Azari-Dorcheh, K.; Vaghefi, S.M. Wear behavior of electroless Ni-P-B₄C composite coatings. *Wear* **2006**, *260*, 123–127. [[CrossRef](#)]
12. León-Patiño, C.; García-Guerra, J.; Aguilar-Reyes, E. Tribological characterization of heat-treated Ni-P and Ni-P-Al₂O₃ composite coatings by reciprocating sliding tests. *Wear* **2019**, *426*, 330–340. [[CrossRef](#)]
13. Wang, S.; Huang, X.; Gong, M.; Huang, W. Microstructure and mechanical properties of Ni-P-Si₃N₄ nanowire electroless composite coatings. *Appl. Surf. Sci.* **2015**, *357*, 328–332. [[CrossRef](#)]
14. Dhakal, D.R.; Kshetri, Y.K.; Gyawali, G.; Kim, T.-H.; Choi, J.-H.; Lee, S.W. Understanding the effect of Si₃N₄ nanoparticles on wear resistance behavior of electroless Nickel-Phosphorus coating through structural investigation. *Appl. Surf. Sci.* **2021**, *541*, 148403. [[CrossRef](#)]
15. Yuxin, W.; Xin, S.; Shanghai, W.; Chuming, L.; Wei, G.; RA, S.; Ramazan, K. Duplex Ni-P-ZrO₂/Ni-P electroless coating on stainless steel. *J. Alloys Compd.* **2015**, *630*, 189–194. [[CrossRef](#)]
16. Sivandipoor, I.; Ashrafizadeh, F. Synthesis and tribological behaviour of electroless Ni-P-WS₂ composite coatings. *Appl. Surf. Sci.* **2012**, *263*, 314–319. [[CrossRef](#)]

17. Sumi, V.; Sha, M.A.; Arunima, S.; Shibli, S. Development of a novel method of NiCoP alloy coating for electrocatalytic hydrogen evolution reaction in alkaline media. *Electrochim. Acta* **2019**, *303*, 67–77. [[CrossRef](#)]
18. Muraliraja, R.; Sudagar, J.; Elansehian, R.; Raviprakash, A.V.; Dhinakaran, R.; Shaisundaram, V.S.; Chandrasekaran, M. Estimation of Zwitterionic Surfactant Response in Electroless Composite Coating and Properties of Ni–P–CuO (Nano) Coating. *Arab. J. Sci. Eng.* **2019**, *44*, 821–828. [[CrossRef](#)]
19. Taye, D.; Mohanty, S.; Das, A.K.; Singh, N.K. Electroless Ni–Al₂O₃–WS₂ Composite Coating on Aluminum Substrate. *Trans. Indian Inst. Met.* **2019**, *72*, 2281–2292. [[CrossRef](#)]
20. Chinchu, K.; Riyas, A.; Sha, M.A.; Geethanjali, C.; Saji, V.S.; Shibli, S. ZrO₂–CeO₂ assimilated electroless Ni–P anti-corrosion coatings. *Surf. Interfaces* **2020**, *21*, 100704. [[CrossRef](#)]
21. Nemane, V.; Chatterjee, S. Evaluation of microstructural, mechanical, and tribological characteristics of Ni–B–W–SiC electroless composite coatings involving multi-pass scratch test. *Mater. Charact.* **2021**, *180*, 111414. [[CrossRef](#)]
22. Holmberg, K.; Laukkanen, A.; Ghabchi, A.; Rombouts, M.; Turunen, E.; Waudby, R.; Suhonen, T.; Valtonen, K.; Sarlin, E. Computational modelling based wear resistance analysis of thick composite coatings. *Tribol. Int.* **2014**, *72*, 13–30. [[CrossRef](#)]
23. Parsazadeh, M.; Fisher, G.; McDonald, A.; Hogan, J.D. Computational modelling of the effect of microstructure on the abrasive wear resistance of tungsten-carbide nickel composite coatings under sub-critical cyclic impact loading. *Ceram. Int.* **2022**, *48*, 14338–14348. [[CrossRef](#)]
24. Jamari, J.; Ammarullah, M.I.; Santoso, G.; Sugiharto, S.; Supriyono, T.; Permana, M.S.; Winarni, T.I.; van der Heide, E. Adopted Walking Condition for Computational Simulation Approach on Bearing of Hip Joint Prosthesis: Review over the Past 30 Years. *Heliyon* **2022**, *8*, e12050. [[CrossRef](#)] [[PubMed](#)]
25. Ren, Q.; Cui, G.; Li, T.; Hassani, M.; Liu, Y.; Kou, Z. High-temperature wear behavior of cobalt matrix composites reinforced by LaF₃ and CeO₂. *Tribol. Lett.* **2021**, *69*, 149. [[CrossRef](#)]
26. Donnet, C.; Erdemir, A. Solid lubricant coatings: Recent developments and future trends. *Tribol. Lett.* **2004**, *17*, 389–397. [[CrossRef](#)]
27. Torres, H.; Ripoll, M.R.; Prakash, B. Tribological behaviour of self-lubricating materials at high temperatures. *Int. Mater. Rev.* **2018**, *63*, 309–340. [[CrossRef](#)]
28. Li, Z.; Wang, J.; Lu, J.; Meng, J. Tribological characteristics of electroless Ni–P–MoS₂ composite coatings at elevated temperatures. *Appl. Surf. Sci.* **2013**, *264*, 516–521. [[CrossRef](#)]
29. Du, S.; Li, Z.; He, Z.; Ding, H.; Wang, X.; Zhang, Y. Effect of temperature on the friction and wear behavior of electroless Ni–P–MoS₂–CaF₂ self-lubricating composite coatings. *Tribol. Int.* **2018**, *128*, 197–203. [[CrossRef](#)]
30. Ürdem, Ş.; Duru, E.; Algül, H.; Uysal, M.; Akbulut, H. Evaluation of high temperature tribological behavior of electroless deposited NiB–Al₂O₃ coating. *Wear* **2021**, *482*, 203960. [[CrossRef](#)]
31. Tyagi, R.; Das, A.; Mandal, A. Electrical discharge coating using WS₂ and Cu powder mixture for solid lubrication and enhanced tribological performance. *Tribol. Int.* **2018**, *120*, 80–92. [[CrossRef](#)]
32. Kundu, S.; Das, S.K.; Sahoo, P. Properties of electroless nickel at elevated temperature—a Review. *Procedia Eng.* **2014**, *97*, 1698–1706. [[CrossRef](#)]
33. Hasan, A.; Mehmet, U.; Ahmet, A. A comparative study on morphological, mechanical and tribological properties of electroless NiP, NiB and NiBP coatings. *Appl. Surf. Sci. Adv.* **2021**, *4*, 10089. [[CrossRef](#)]
34. Apachitei, I.; Tichelaar, F.D.; Duszczyc, J.; Katgerman, L. The effect of heat treatment on the structure and abrasive wear resistance of autocatalytic NiP and NiP–SiC coatings. *Surf. Coat. Technol.* **2002**, *149*, 263–278. [[CrossRef](#)]
35. Buchtfk, M.; Doskočil, L.; Brescher, R.; Doležal, P.; Másilko, J.; Wasserbauer, J. The Effect of Crystallization and Phase Transformation on the Mechanical and Electrochemical Corrosion Properties of Ni–P Coatings. *Coatings* **2021**, *11*, 447. [[CrossRef](#)]
36. Balaraju, J.N.; Narayanan, T.S.N.S.; Seshadri, S.K. Structure and phase transformation behaviour of electroless Ni–P composite coatings. *Mater. Res. Bull.* **2006**, *41*, 847–860. [[CrossRef](#)]
37. Uysal, M. Electroless codeposition of Ni–P composite coatings: Effects of graphene and TiO₂ on the morphology, corrosion, and tribological properties. *Metall. Mater. Trans.* **2019**, *50*, 2331–2341. [[CrossRef](#)]
38. Ni, M.; Wang, S.; Li, W.; Huang, W. A novel self-lubricating Ni–P–AlN–WS₂ nanocomposite coating. *Mater. Res. Express* **2019**, *6*, 116413. [[CrossRef](#)]
39. Gültekin, D.; Duru, E.; Akbulut, H. Improved wear behaviors of lead-free electroless NiB and Ni–B/CeO₂ composite coatings. *Surf. Coat. Technol.* **2021**, *422*, 127525. [[CrossRef](#)]

Disclaimer/Publisher’s Note: The statements, opinions and data contained in all publications are solely those of the individual author(s) and contributor(s) and not of MDPI and/or the editor(s). MDPI and/or the editor(s) disclaim responsibility for any injury to people or property resulting from any ideas, methods, instructions or products referred to in the content.